Frank Ernst, Michael W. Finnis*, Ansgar Koch, Camilla Schmidt, Boris Straumal, and Wolfgang Gust**

(Max-Planck-Institut für Metallforschung, Institut für Werkstoffwissenschaft, Seestraße 92, D-70174 Stuttgart, Germany; *Atomistic Simulation Group, School of Mathematics and Physics, Queen's University of Belfast, BT7 1NN, Ireland; **Universität Stuttgart, Institut für Metallkunde, Seestraße 75, D-70174 Stuttgart, Germany)

Structure and Energy of Twin Boundaries in Copper

This article presents the results of experimental and theoretical studies on the energy and structure of $\Sigma3$ tilt boundaries with $\langle 110 \rangle$ and $\langle 211 \rangle$ tilt axis in Cu. For both types of boundaries, a plot of the grain boundary energy versus the inclination of the boundary plane features a minimum at high inclinations against the plane of the coherent twin boundary. Along with this second energy minimum, the boundaries exhibit complex, three-dimensional struc-tures, featuring a thin slab along the boundary plane in which Cu adopts unusual crystal structures. In the $\langle 110 \rangle$ tilt boundaries the slab has a rhombohedral structure (9R), while in the $\langle 211 \rangle$ tilt boundaries it has a body-centered cubic structure. These structures seem to be energetically favorable because they continue close-packed layers of atoms across the grain boundary.

Struktur und Energie von Zwillingsgrenzen in Kupfer

Diese Arbeit schildert die Ergebnisse experimenteller und theoretischer Untersuchungen zur Energie und Struktur von $\Sigma3$-Kippkorngrenzen mit $\langle 110 \rangle$- und $\langle 211 \rangle$-Kippachse in Kupfer. Trägt man die Korngrenzenenergie gegen den Neigungswinkel der Korngrenzenebene auf, so zeigen bei-de Typen ein Energieminimum bei hohen Neigungswin-keln gegen die Ebene der kohärenten Zwillingsgrenze. In Verbindung mit diesem Energieminimum bilden sich komplexe, dreidimensionale Korngrenzenstrukturen. Da-bei entsteht entlang der Korngrenzenebene eine dünne Schicht, in der das Kupfer ungewöhnliche Kristallstruktu-ren annimmt. Bei den $\langle 110 \rangle$-Kippkorngrenzen hat die Schicht eine rhomboedrische Struktur (9R), bei den $\langle 211 \rangle$-Kippkorngrenzen dagegen eine kubisch-raumzen-trierte Struktur. Es scheint, daß diese Strukturen besonders energiegünstig sind, weil sie dichtgepackte Atomlagen über die Korngrenze hinweg fortsetzen.

1 Introduction

The relevant macroscopic properties of many polycrystal-line materials depend to a large extent on the nature of the grain boundaries. Grain boundaries influence materials properties like mechanical strength, plasticity, or electrical conductivity. Moreover, grain boundaries play an important role for solid state reactions in crystalline materials. For example, grain boundaries may enhance low temperature diffusion, cause segregation of impurities, control texture formation, or serve as nucleation sites for precipitates. Therefore, understanding materials properties and behav-ior requires research on grain boundaries.

The two most fundamental aspects of a grain boundary are its structure (atom coordinates) and its energy (excess Gibbs energy). Grain boundary structure and grain bound-ary energy, however, are closely interrelated: The structure determines the energy of the grain boundary, while the en-ergy 'selects' the most favorable structure – according to the laws of thermodynamics.

To describe the crystallography of a planar grain bound-ary at macroscopic level, one needs to determine five param-eters [1, 2]: three parameters to describe the orientation re-lationship between the two grains and two parameters to determine the inclination of the boundary plane. It has been realized early that grain boundaries with extreme prop-erties (minimum energy, maximum mobility, etc.) often have a 'special' crystallography [1, 2]. Many observations have confirmed that 'special' grain boundaries result if the two grains have an orientation relationship corresponding to a coincidence site lattice with a small unit cell [3]. This implies that the lattices of the two grains, when translated to coincide at their origin, have a high density $1/\Sigma$ of com-mon sites. While the effect of the orientation relationship on grain boundary properties is well established theoretically [4 to 10] as well as experimentally [11 to 14], only few studies have dealt with the influence of grain boundary in-clination (for example, see references [15 to 19]. The reason for this deficiency has to do with the experimental difficul-ties in guessing the inclination of a grain boundary from its intersection line with a polished surface. Even when imag-ing the interior of the material by TEM (transmission elec-tron microscopy) it remains difficult to determine the incli-nation of an arbitrary grain boundary.

A rewarding although laborious approach to investigate the effect of boundary inclination consists of fabricating a series of macroscopic bicrystals with constant orientation relationship and systematic variation of the inclination. Using this approach, we have studied the influence of boundary inclination on the structure and energy of twin boundaries in Cu [18 to 25]. More precisely, the grain boundaries we have fabricated and studied so far belong to two different series of $\Sigma 3$ tilt boundaries. Figure 1 illustrates their crystallography. In both series of boundaries we have successively tilted the boundary plane against the {111} plane of the coherent twin boundary, while keeping the $\Sigma 3$ orientation relationship constant. The $\Sigma 3$ orientation relationship corresponds to a 71° ⟨110⟩ or 180° ⟨211⟩ rotation of one lattice with respect to the other. In our first series of $\Sigma 3$ tilt boundaries the tilt axis corresponds to the common ⟨110⟩ direction of the two grains, while in the second series the tilt axis corresponds to the common ⟨211⟩ direction.

Our studies include experimental and theoretical work. Using thermal grooving experiments we have determined

Figs. 1a to f. Crystallography of $\Sigma 3$ tilt boundaries in Cu. (a) Coherent twin boundary (b) Definition of the tilt angle ϕ_{110} characterizing $\Sigma 3$ ⟨110⟩ tilt boundaries. (c) $\Sigma 3$ 82° ⟨110⟩ tilt boundary. According to the results of thermal grooving experiments and numerical structure calculations this boundary has a structure of minimum energy. (d) $\Sigma 3$ 90° ⟨110⟩ tilt boundary, sometimes denoted as 'symmetrical incoherent' twin boundary. (e) Definition of the tilt angle ϕ_{211} characterizing $\Sigma 3$ ⟨211⟩ tilt boundaries. (f) $\Sigma 3$ 84° ⟨110⟩ tilt boundary. According to the results of thermal grooving experiments and numerical structure calculations this boundary has a structure of minimum energy.

the energies of these boundaries. By means of QHRTEM (quantitative high resolution transmission electron microscopy) we have determined the atom positions at several twin boundaries with high precision. Both kinds of experimental observations have been compared with results obtained by numerical structure and energy calculations (computer modeling). For the latter we have employed empirical many-body potentials.

In this paper, we summarize our work on the structure and energy of individual twin boundaries in Cu. While previous publications have dealt with special results and technical details of the individual experimental and theoretical methods, this paper provides a comprehensive overview on the structure and energy of twin boundaries in Cu.

2 Experimental Procedures and Techniques

2.1 Fabrication of Cu Bicrystals

For the experimental studies we have fabricated Cu bicrystals by diffusion bonding of oriented single crystal slabs in high vacuum. The slabs were cut from Cu single crystals, which we had grown from 99.999 wt.% Cu ingot by the Bridgman technique [26]. The slabs had a thickness of 0.5 mm, a length of 5 mm, and a width of 10 mm. Prior to diffusion bonding we polished the bonding surfaces with an ultra mill until the roughness was no more than 10 nm. Subsequently, we cleaned the polished surfaces in high-purity acetone. After adjusting the orientation relationship we loaded the slabs into Mo crucibles and bonded them at 1313 K (97 % of the melting temperature T_m) at a total atmospheric pressure below 10^{-5} Pa. After bonding, we equilibrated the boundary structure by annealing the bicrystals at 1173 K for 15 h.
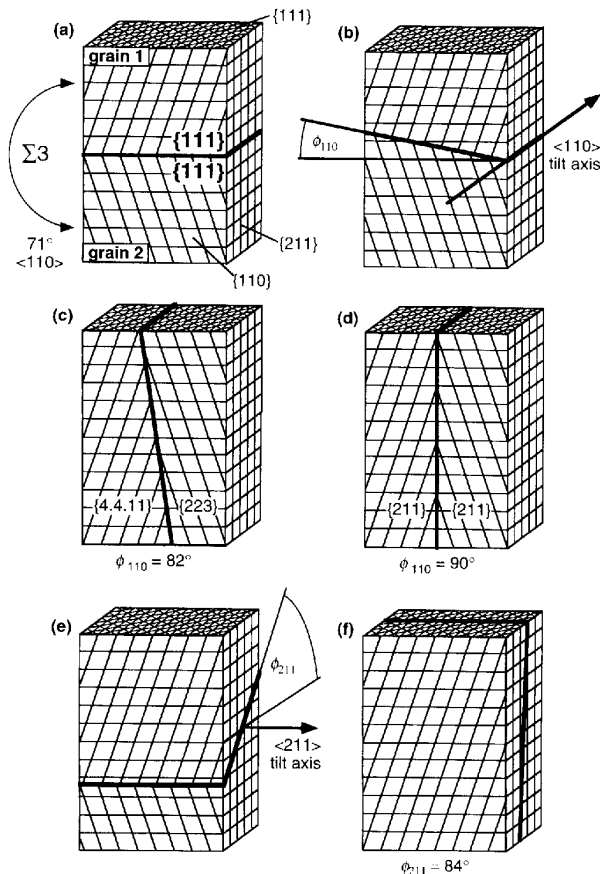
2.2 Measurements of Grain Boundary Energies

Using a spark erosion machine, we cut 2 mm slabs from the bicrystals normal to the tilt axis. On these specimens we performed thermal grooving experiments to determine the grain boundary energy relative to the energy of the slab surface ({110} or {211}). When annealing a grain boundary intersecting with a polished surface at sufficiently high temperature (> 0.5 T_m) the surface forms a groove to equilibrate the tension of the grain boundary with the tension of the surface. Figure 2 illustrates the geometry of such a groove. In thermal equilibrium the forces corresponding to the tensions γ_1, γ_2 and γ_b balance at the bottom of the groove, and the two sides of the groove make a characteristic angle $\Psi = \Psi_1 + \Psi_2$. While Ψ remains constant, the groove depends by evaporation or surface diffusion [27].

Since we consider a single component system near the melting point the two tensions represent the energy of the corresponding Cu surface and the energy of the grain boundary, respectively [28]. Neglecting the influence of Herring torque terms [29], and approximating $\gamma_1 = \gamma_2 =: \gamma_s \Rightarrow \Psi_1 \approx \Psi_2 =: \Psi$ in Fig. 2 we obtain

$$\frac{\gamma_b}{\gamma_s} = 2\cos[\Psi] \tag{1}$$

Thus, by measuring the angle Ψ we can determine the energy γ_b of the grain boundary relative to the energy γ_s
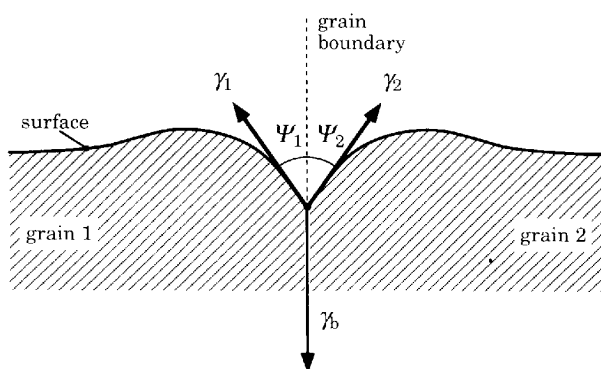
Fig. 2. Geometry of a thermal groove forming where a grain boundary intersects with the polished surface of a Cu bicrystal. Because the surface energy of Cu does not exhibit pronounced anisotropy, we approximate $\gamma_2 = \gamma_1 =: \gamma_s$ and, consequently, $\Psi_2 - \Psi_1 -: \Psi$. By means of interference light microscopy we measure the angle Ψ to obtain the ratio between grain boundary energy γ_b and surface energy γ_s through the relation (1).

of the surface. To measure the angles we image the groove in a light microscope equipped with a monochromatic sodium light source and a Michelson two-beam interferometer. The interference pattern the reflected beam forms with the reference beam exhibits characteristic distortions representing the depth profile of the groove. By recording the pattern together with a scale we obtain the relative positions of intensity minima and maxima along the x direction (normal to the groove). To evaluate these data we assume that the depth profile on each side of the groove can be described by a second order polynomial in x. A computer program performing a least-squares fit to the experimental data serves to determine the best-matching polynomials. Before carrying out the least-squares fit the program corrects for artefacts originating from the large aperture of the objective lens [30].

2.3 TEM Sample Preparation and Microscopy

From the Cu bicrystals described in Section 2.1 we also prepared the TEM samples for imaging along the respective direction of the tilt axis (either $\langle 110 \rangle$ or $\langle 211 \rangle$). By means of spark erosion we first cut 0.3 mm slices normal to the tilt axis. After grinding the slices down to a thickness of about 80 μm (using SiC paper), we punched out 3 mm discs with the boundary traversing the discs center. Finally, we thinned the central region of the disc to electron transparency by electro-polishing in an electrolyte of 33 % nitric acid and 67 % methanol.

To image the structure of the grain boundaries in $\langle 110 \rangle$ and $\langle 211 \rangle$ projection we employed a JEM-ARM 1250 high-voltage high-resolution transmission electron microscope (JEOL). Operating at an accelerating voltage of 1250 kV, this microscope provides a point resolution of 0.105 nm with its top-entry objective lens and 0.120 nm with its side-entry lens [31]. Both resolution limits suffice to resolve the {111}, {200}, and {220} planes of Cu (compare Fig. 1).

First we recorded the images on photographic plates. Subsequently, for the purpose of quantitative evaluation of image intensities, we digitized the images by scanning the negatives with a diode array scanner (Eikonix) provid-

ing a dynamic range of 12 bit. The codes for the optimization program and the quantitative image comparison have been written in interactive data language (IDL) and executed on DEC-alpha workstations. For image simulations we use the software package 'EMS' [32].

2.4 Structure Determination by Quantitative Image Analysis

Interpreting HRTEM images of a grain boundary in edge-on orientation 'naively', in terms of the projected interface structure, may lead to errors. In general, dynamic electron diffraction in the sample and aberrations of the electron optics complicate the relationship between the image wave $\Psi_i[x]$ and the structure of the sample. Moreover, in conventional HRTEM imaging the photographic film or camera in the image plane only records the intensity of the electron wave, rather than its amplitude and phase. For these reasons, there is no straight-forward way to reconstruct the structure of an arbitrary specimen from its HRTEM image. In particular, the above complications may destroy the intuitively expected correspondence between the image pattern and the positions of atoms columns in the specimen.

The most common method to avoid artefacts in the interpretation of HRTEM images relies on image simulations. After proposing a number of different models for the atomistic structure of the interface one calculates the corresponding HRTEM images on a computer. The model that yields the best-matching image simulation presumably represents the best approximation for the real structure of the specimen. Usually, a human observer compares simulated and experimental images by mere visual inspection. Obviously, this method leads to vague conclusions because the result of visual analysis will depend on the individual nature of the observer. In particular, the observer cannot quantify discrepancies between simulated and experimental image.

Consequently, it remains impossible to quantify error limits for the structure with the best-matching simulated image.

In our studies of twin boundary structures in Cu we have overcome these limitations through quantitative evaluation of image intensities [20, 21, 23, 33 to 35]. Such quantitative HRTEM comprises digitization of HRTEM images and numerical processing with well-defined algorithms. Starting from a preliminary model, numerical refinement procedures automatically determine the structure with the best-matching image simulation. Moreover, we can quantify the reliability of the 'refined' grain boundary structure obtained in this way.

Our procedure of quantitative image analysis consists of three steps [21]: First, we reduce the noise in the experimental image. This is done by averaging over several (typically five) repeat units along the grain boundary, or by adaptive Fourier filtering [36]. In the second step we cross-correlate one repeat unit of the image with the pattern of a single column of Cu atoms. Assuming that a Cu column resides at each maximum of the cross-correlation image we obtain a preliminary model for the repeat unit of the boundary structure. However, this model does not account for potential artefacts of the HRTEM image. In the third step, therefore, we refine the preliminary model in an iterative procedure. A single loop of this procedure includes simulating the

HRTEM image of the current model, comparing the image quantitatively (numerically) with the experimental image, and improving the model according to the results of the image comparison.

To quantify the discrepancy between (simulated and experimental) images, one may regard them as vectors of pixel intensities and calculate the euclidean distance between the vectors. In this case, however, the distance depends on the format (number of pixels) of the images. To avoid this dependence we employ the 'normalized euclidean distance' (NED). For two images A and B the NED has the form

$$D(A,B) = \frac{\| A - B \|}{\sqrt{\| A \| \cdot \| B \|}} \qquad (2)$$

where $\| \ldots \|$ denotes the euclidean length.

The iterative refinement yields the refined structure of the grain boundary. The simulated image of this structure yields the best match with the experimental image being evaluated. Thus, we assume that the refined structure constitutes the best model for the real boundary structure.

Numerically, we can determine the column positions in the refined structure to any desired precision. However, there is only a finite reliability by which these positions represent the true column positions. The limitation of the reliability originates from the following problem [21]: Even if we knew the real structure precisely, image discrepancy D^* always persists between experimental and simulated image because image simulations do not account for a number of factors influencing the experimental HRTEM image: oxides or contaminants on the specimen surface, inelastic electron scattering, slight misalignments, and the like. Moreover, the experimental image contains residual noise. As a consequence of these effects, we can safely distinguish two different structures only if their image vectors differ by more than D^*.

Thus, to estimate the reliability of the refined structure we need to explore the extent to which one may modify the refined structure without changing its simulated image by more than D^*. For this purpose we modify the refined structure in a well-defined manner and investigate the corresponding change of the simulated HRTEM image.

In practice, we displace the columns of the refined structure into random directions by distances randomly drawn from a Gauß distribution with a standard deviation σ. Then we simulate the image of the modified structure and calculate its NED to the simulated image of the refined structure. Repeating this for many different standard deviations σ we obtain a graph $D[\sigma]$ correlating image discrepancy (NED) with structure discrepancy (standard deviation of column displacements). Reading the abscissa corresponding to the ordinate D^* we obtain the average reliability of the column positions [21, 22, 33].

2.5 Computer Modeling of Grain Boundary Structures

To model the structures of the twin boundaries, we simulated the relaxation of atom positions near the boundary plane in an orthorhombic simulation cell, imposing periodic boundary conditions. In these numerical structure calculations we described the interaction between the Cu atoms by empirical many-body potentials of embedded-

atom [37] or Finnis–Sinclair [38, 40] type. With these potentials we performed molecular statics as well as molecular dynamics calculations. In molecular statics calculations one minimizes the total energy of the system by displacing the atoms in an iterative cycle; we have used a variant of the method of steepest descents. The results of such calculations refer to a temperature of 0 K.

While molecular statics calculations only include the forces on the atoms, molecular dynamics calculations also include the momentum of each atom. This allows us to model the system at a finite temperature. Moreover, molecular dynamics can overcome potential barriers, provided that these are not too high. Compared to molecular statics calculations, however, molecular dynamics calculations demand more computing power. The size of the simulation cell and the computer system available impose an upper limit for the time interval over which one may follow the relaxation with such calculations. In the calculations we have carried out for Cu twin boundaries, such time interval has the order of only a few hundred picoseconds. This time interval suffices, however, to anneal starting structures into stable structures.

3 Twin Boundaries with $\langle 110 \rangle$ Tilt Axis

3.1 Measured and Calculated Grain Boundary Energies

Figure 3 presents our data on the energy of $\Sigma 3$ $\langle 110 \rangle$ tilt boundaries versus the inclination angle ϕ_{110} [17 to 19]. The data points with error bars represent experimental data obtained by thermal grooving experiments, while the other points refer to molecular statics calculations. The calculated energies are up to 10 % larger that the measured energies. The discrepancy may originate from two possible reasons. First, the calculated energies have been normalized with the energy of the (110) surface as calculated by molecular statics ($\gamma_{110} = 1.42 \text{ J/m}^2$ [41]), and deviations from the real value will introduce discrepancies with the experimental data of the relative grain boundary energies. It is well known that semi-empirical many body
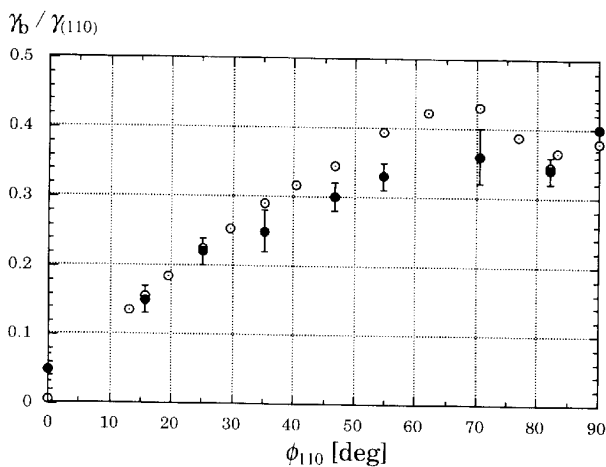

Fig. 3. Energy γ_b of $\Sigma 3$ $\langle 110 \rangle$ tilt boundaries versus the inclination angle ϕ_{110} [18, 19] (energy data in units of γ_{110}, the energy of the Cu (110) surface). The data points with error bars represent experimental data obtained by thermal grooving experiments, while the other points refer to molecular statics calculations.

potentials tend to underestimate the surface energy. Second, experimental problems of measuring the depth of the thermal groove tend to make grain boundary energies appear smaller than they really are [42]. Nevertheless, the two sets of data agree well and predict the same form of the $\gamma_b[\phi_{110}]$ curve: The boundary energy has a deep minimum at $\phi_{110} = 0$, which corresponds to the coherent twin boundary. With increasing inclination ϕ_{110} the energy first rises quickly and then approaches a plateau at 60°. Both, experimental and theoretical data exhibit a second energy minimum. Remarkably, this minimum does not occur at the inclination $\phi_{110} = 90°$ of the symmetrical incoherent twin boundary but occurs at $\phi_{110} = 82°$. The minimum is less deep and less pronounced than the minimum at $\phi_{110} = 0°$.

Computer modeling and HRTEM imaging have revealed that the grain boundaries in the vicinity of the second minimum of the $\gamma_b[\phi_{110}]$ curve have a non-trivial structure, featuring a thin slab of Cu with a rhombohedral structure along the boundary [18, 19]. The following two sections deal with the details of this grain boundary structure.

3.2 Structures Predicted by Computer Modeling

To calculate the structures and energies of the Σ3 ⟨110⟩ tilt boundaries we have used a molecular statics algorithm. To describe the interatomic interaction, we first employed an embedded-atom potential of the type introduced by Foiles, Daw, and Baskes [37]. Because this potential predicts unphysically low energies for stacking faults and for the coherent twin boundary, we repeated our calculations with potentials of the Finnis-Sinclair type [38 to 40]. No significant differences were found, but for subsequent work on the boundaries of the ⟨211⟩ tilt axis (Sections 4.1 and 4.2) we used the potentials of Foreman et al. [39], since they had been fitted to give an acceptable stacking fault energy as well as to predict the experimentally observed lattice parameter and elasticity constants.

Because the algorithm we used for molecular statics cannot overcome barriers in the potential, we have tried many starting configurations to ensure that we identify the most stable structure. The starting configurations we have tried differ with respect to the number of atoms in the simulation cell and with respect to the translation state (the rigid body translation characterizing the relative positions of the two grains).

Figures 4 and 5 depict the structures of the 82°⟨110⟩ and the 90°⟨110⟩ tilt boundary as obtained by molecular statics calculations [43]. For both inclinations, the boundary has the following characteristic features: (i) The boundary constitutes a three-dimensional slab rather than a two-dimensional disturbance of the crystal structure. The slab has a thickness of about 1 nm. (ii) The two sets of {111} planes that lying parallel to each other in the two grains exhibit a lateral offset (parallel to the boundary plane). The offset amounts to 0.2 nm, which roughly corresponds to the distance d_{111} between neighboring {111} planes in fcc (face-centered cubic) Cu. Because of this offset the close-packed layers crossing the boundary slab feature a smooth bending. (iii) The slab forms two different types of interfaces with the adjacent Cu grains. One interface (on the left in Figs. 4 and 5) corresponds to a small angle boundary consisting of Shockley partial dislocations in every third close-packed layer normal to the boundary plane. The other interface con-
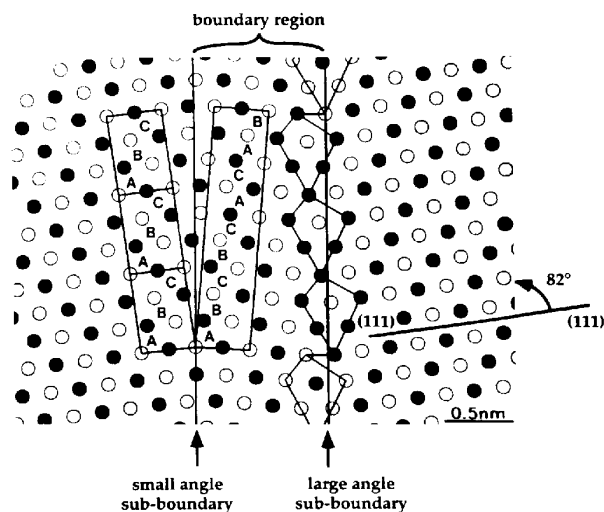

Fig. 4. Structures of the Σ3 82° ⟨110⟩ tilt boundary as obtained by molecular statics calculations [18, 19, 41]. The viewing direction corresponds to the direction of the tilt axis, a common ⟨110⟩ direction of the two grains. White and black spots indicate atoms in a and b layers of the stacking sequence ...abab... of {110} layers along this ⟨110⟩ direction.

sists of kite-shaped structural units and we refer to it as the large angle boundary. (iv) The stacking sequence of close-packed layers in the boundary slab corresponds to

$$...abcbcacab...\qquad(3)$$

This stacking sequence characterizes a structure with rhombohedral symmetry. In Pearson's notation the structure is denoted as Sm [44]. Since the period normal to the 3-fold axis includes 9 close-packed layers, we denote this structure by 9R. The standard fcc structure of Cu, in contrast, corresponds to 3C in this nomenclature (in Pearson's notation: A1). Analysis of stacking sequences using an Ising or Ždahnov [45] representation reveals that after the fcc structure of Cu and a hypothetical hcp (hexagonal close-
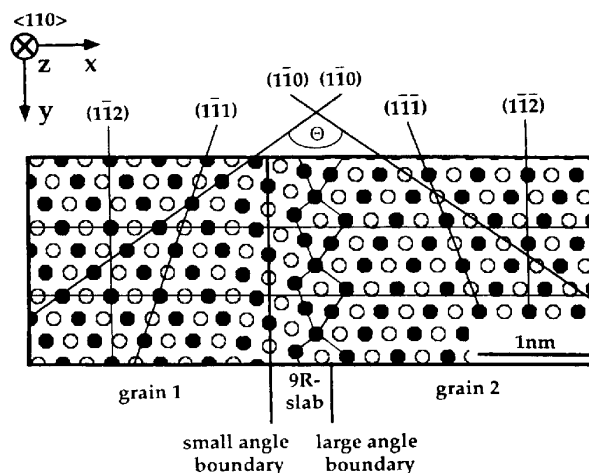

Fig. 5. Structure of the Σ3 90° ⟨110⟩ tilt boundary as obtained by molecular statics calculations [18, 19, 41]. The presentation corresponds to Fig. 4. Note that the period of this boundary equals only one third the period of the Σ3 82° ⟨110⟩ tilt boundary.

packed) structure (see section 4.2) the 9R structure corresponds to the next simplest stacking pattern of close-packed layers [43].

3.3 Structures Observed by HRTEM

Experimental HRTEM images of Σ3 ⟨110⟩ tilt boundaries confirm the existence of a 9R slab [18, 19, 21, 22]. For example, Figure 6 presents a high resolution image of the 82 ⟨110⟩ tilt boundary, recorded in the JEM-ARM 1250. This incident electron beam was parallel to the ⟨110⟩ tilt axis common to the two grains. The image belongs to a through-focus series and was recorded at 30 nm underfocus, which is close to the Scherzer focus of the JEM-ARM 1250. Under these conditions the positions of projected atomic columns coincide with the dark spots.

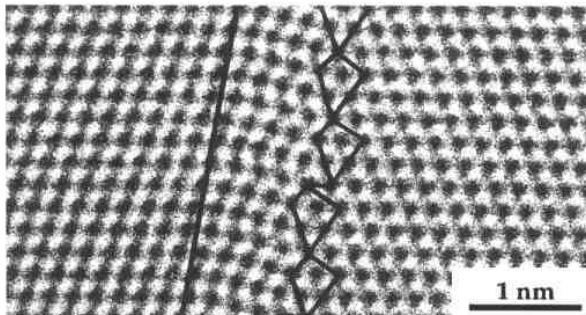The grain boundary passes vertically through each image. The lines overlaid with the HRTEM images indicate

Fig. 6. Experimental HRTEM image of the Cu Σ3 82 ⟨110⟩ tilt boundary (see Figs. 1c and 4) in ⟨110⟩ projection. The image has been recorded in the Stuttgart atomic resolution microscope ARM 1250 (top-entry lens), which achieves a point resolution of 0.105 nm [8]. In regions of bulk Cu the black spots coincide with the positions of atom columns. The image reveals a thin slab of 9R structure, which relates to the standard fcc structure of Cu (3C) by introducing a stacking fault on every third {111} plane.
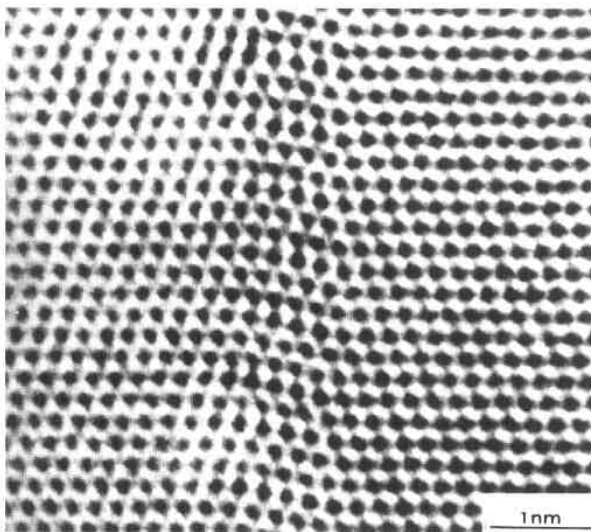

Fig. 7. Experimental HRTEM image of the Cu Σ3 90 ⟨110⟩ tilt boundary (see Figs. 1d and 5), recorded under the same conditions as the image in Fig. 6.
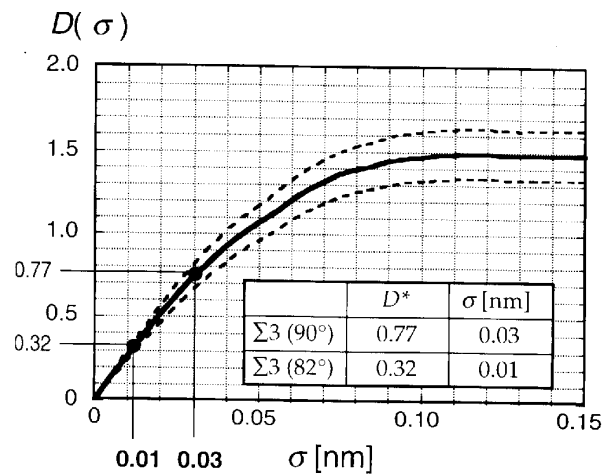
$D(\sigma)$

	D^*	σ [nm]
Σ3 (90°)	0.77	0.03
Σ3 (82°)	0.32	0.01

Fig. 8. For the HRTEM images of the Σ3 ⟨110⟩ tilt boundaries with 9R structure, this graph translates image discrepancies (NED) into structural discrepancies (standard deviation σ of column shifts). The dotted graphs characterize the scattering for constant σ.

the nature and the position of the structural units in the large angle boundary, as well as the position of the small angle boundary. The periodic unit of the large angle boundary consists of three kite-shaped structural units and a microfacet of coherent twin boundary parallel to {111}. The width w of the 9R zone in-between amounts to $w = 2.5\ a_{Cu}$ where $a_{Cu} = 0.3615$ nm denotes the lattice parameter of Cu. Qualitatively, the experimentally observed structure agrees well with the molecular statics model in Fig. 4.

Figure 7 presents the corresponding image for the 90 ⟨110⟩ tilt boundary. Like Fig. 6 this image has been recorded close to Scherzer focus, thus the atom columns appear as dark spots.

We have used the images of Figs. 6 and 7 to analyze in detail the structure of the corresponding grain boundaries [21, 22]. For the 90 and the 82 boundary the residual image discrepancy D^* amounts to 0.77 and 0.32, respectively. From Fig. 8 we learn that these values correspond to column displacements with a standard deviations of 0.03 and 0.01 nm, respectively. Thus, the average uncertainty of the column positions in the repeat unit has the order of a few tenths of an Ångstrom. Error analysis of every single column position in the repeat unit by an independent method [9, 10] has revealed that the largest uncertainties occur in the 9R region. Even here, however, the errors do not exceed 0.025 nm.

Figure 9 presents the results of the structure refinement and compares them with the predictions of the molecular statics calculations. In both figures we have aligned the theoretical and the experimental positions in the top left corner. Figure 9a refers to the 82 ⟨110⟩ tilt boundary. The drawing reveals an excellent agreement between the refined structure and the prediction of molecular statics calculations. In regions of bulk Cu there is perfect agreement. In the 9R region of the boundary, only small discrepancies of less than 0.05 nm occur between the theoretical and the experimental column positions. Still, these discrepancies are significant because they exceed the above error limits of 0.01 nm on the average and 0.025 nm in the 9R zone.

For the 90° ⟨110⟩ tilt boundary, Fig. 9b exhibits good agreement between theory and experiment on the left side of the boundary. In the 9R region and on the right side of the boundary we observe deviations of up to ≈ 0.05 nm. While these deviations are small, they exceed the above error limit of 0.03 nm, and thus we consider them as significant. On the right side of the boundary the streaks indicating the mismatch between theory and experiment have approximately the same size and direction. This means that theory and experiment disagree on the rigid body shift between the two grains. The theory overestimates the expansion normal to the boundary plane and underestimates the lateral offset, which breaks the mirror symmetry.

Table 1 summarizes the global differences between the models obtained by molecular statics calculations and the experimentally determined structures [46].

4 Twin Boundaries with ⟨211⟩ Tilt Axis

4.1 Measured and Calculated Grain Boundary Energies

Figure 10 depicts the experimental and theoretical energies we have obtained for Σ3 ⟨211⟩ tilt boundaries [24, 25, 47, 48]. At high inclinations the calculations yield energies significantly larger than the measured energies. While the discrepancy appears more pronounced than in Fig. 3 we believe that it occurs for the same reasons – underestimation of the surface energy in molecular statics calculations ($\gamma_{211} = 1.37$ J/m² [41]), or experimental problems of measuring the depth of the thermal grooves.

Still, the theoretical and the experimental data indicate similar dependencies of the grain boundary energy on the inclination ϕ_{211}: The absolute minimum of the energy corresponds to the coherent twin boundary. Similar to Fig. 3, a second minimum occurs at an inclination close to, but not exactly at 90°. In Fig. 10 the calculated energies exhibit

Table 1. Theoretical and experimentally observed properties of Σ3 82° ⟨110⟩ and Σ3 90° ⟨110⟩ tilt boundaries in Cu. $a_{Cu} = 0.3615$ nm denotes the lattice parameter of Cu.

Property	Σ3 82° ⟨110⟩		Σ3 90° ⟨110⟩	
	Theory	Experiment	Theory	Experiment
Expansion normal to boundary plane	$0.05a_{Cu}$	$0.05a_{Cu}$	$0.13a_{Cu}$	$0.04a_{Cu}$
Thickness of 9R layer	$1.71a_{Cu}$	$2.11a_{Cu}$	$1.33a_{Cu}$	$2.53a_{Cu}$
Lateral offset	$0.48a_{Cu}$	$0.48a_{Cu}$	$0.37a_{Cu}$	$0.50a_{Cu}$
Angle between close-packed layers	15.6	12.8	15.4	11.2

a second minimum at $\phi_{211} = 80°$. Apparently, the experimental data does not confirm the existence of such a minimum but rather suggests a plateau for inclinations around 80°. However, both boundaries corresponding to the points left and right of the point at 84° were observed to facet, while the boundary with $\phi_{211} = 84°$ does not facet. Because faceting decreases the average grain boundary energy these observations imply that the thermal grooving experiments, which average over submicron facets, correctly deliver the energy for $\phi_{211} = 84°$, while they underestimate the energies of the two boundaries with slightly smaller or slightly larger inclinations. If these two boundaries were not faceted their energy would be higher and the experimental data in Fig. 10 would possess a second minimum at 84°. Since the results of the molecular dynamics calculations refer to unfaceted boundaries, we conclude that theory and experiment agree well and that the grain boundary energy does have a second minimum at 84° (or 80°).

(a)

(b)
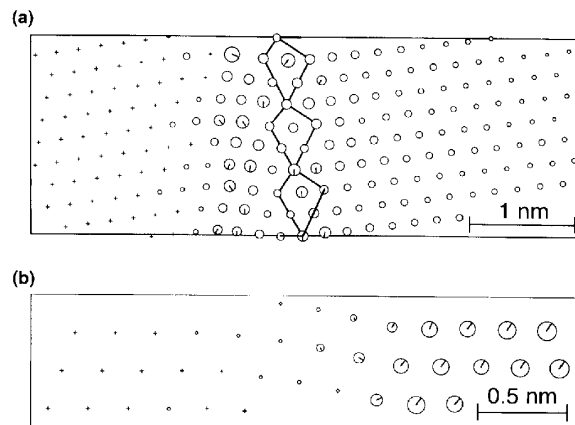
Figs. 9a and b. Comparison between the experimentally determined structure of Σ3 ⟨110⟩ tilt boundaries with the prediction of molecular statics calculations [7]. The centers of the circles mark the column positions determined by QHRTEM, while the theoretical positions correspond to the ends of the streaks pointing away from the centers. Accordingly, the radii of the circles indicate the deviation between theory and experiment. The two sets of positions have been translated such that they coincide in the top left corner. (a) Σ3 82° ⟨110⟩ tilt boundary. (b) Σ3 90° ⟨110⟩ tilt boundary.

$\gamma_b / \gamma_{(211)}$

ϕ_{211} [deg]
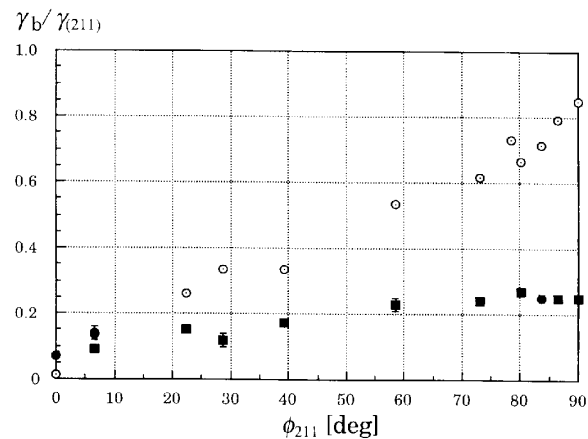
Fig. 10. Energy γ_b of Σ3 ⟨211⟩ tilt boundaries versus the inclination angle ϕ_{211} [24, 25, 47, 48] (energy data in units of γ_{211}, the energy of the Cu ⟨211⟩ surface). The data points with error bars represent experimental data obtained by thermal grooving experiments, while the other points refer to molecular statics calculations. Among the former, circular points correspond to unfaceted boundaries, while rectangular points correspond to faceted boundaries.

4.2 Structures Predicted by Computer Modeling

To calculate the structure of the $\Sigma 3$ 84° $\langle 211 \rangle$ tilt boundary we have employed molecular statics as well as molecular dynamics calculations with simulated temperatures between 500 and 900 K. In both types of calculations we described the interatomic forces by a semi-empirical potential of the Finnis-Sinclair type [38 to 40]. This potential [39] has been fitted to reproduce the lattice parameter and the elasticity constants of Cu single crystals with the fcc structure.

Our molecular dynamics calculations are based on an Andersen-Parrinello-Rahman Lagrangian [49, 50], enabling the simulation cell to vary with respect to volume and shape while the hydrostatic pressure remains constant. In each run we continued the relaxation until the fluctuations of the kinetic and potential energy converged to constant values, which means that equilibrium has been reached. At the end of each calculations we 'quenched' the system to $T \approx 0$K in 4 ps.

Figure 11 presents a ball model of the structure calculated by molecular dynamics [24, 25, 47]. The viewing direction corresponds to the $\langle 211 \rangle$ tilt axis of the grain boundary, and the boundary plane traverses the image from the upper left to the lower right. Similar to the $\Sigma 3$ $\langle 110 \rangle$ tilt boundaries of Figs. 4 and 5 the calculated structure of this boundary exhibits the following features: (i) The boundary constitutes a three-dimensional slab rather than a two-dimensional disturbance of the crystal structure. The slab has a thickness of about 1 nm. (ii) The two sets of {111} planes that lying parallel to each other in the two grains exhibit a lateral offset (parallel to the boundary plane). The offset amounts to

0.2 nm, which roughly corresponds to the distance d_{111} between neighboring {111} planes in fcc Cu. Because of this offset the close-packed layers crossing the boundary slab feature a smooth bending. (iii) Similar to the $\Sigma 3$ $\langle 110 \rangle$ boundaries of Section 3 the material within the boundary slab does not have the standard fcc structure of Cu. Instead, it has the bcc (body-centered cubic) structure of α-Fe (A2 in Pearson's notation [44]).

To visualize the bcc structure of the boundary slab the lower inset in Fig. 11 shows the projected structure of the marked region after rotating it by 45° around an axis parallel to the close-packed layers and parallel to the image plane. The inset shows a structure that corresponds to the structure of α-Fe in $\langle 100 \rangle_{bcc}$ projection. Apart from a small rotation, the {110} planes of the bcc region correspond to the {111} planes of the fcc Cu in the adjacent grains, while the {200}$_{bcc}$ planes correspond to {220}$_{fcc}$.

According to the molecular dynamics calculations the width of the bcc slab increases with increasing temperature. The structure of Fig. 11 corresponds to a temperature of 0 K. At 900 K, however, the calculations predict a wider bcc slab. The width oscillates in time with a period of about 70 ps, which is probably an artifact of the cell-size used in the molecular dynamics simulation. Averaging the width over a time interval of 260 ps (entire simulation) yields two or three times the thickness at room temperature (the exact value depends on the dimensions of the simulation cell [47]). Detailed analysis of the 900 K simulations has indicated that in the central region of the grain boundary slab, the structure is more complicated when the slab is wider. It appears to be a mixture of microscopic regions
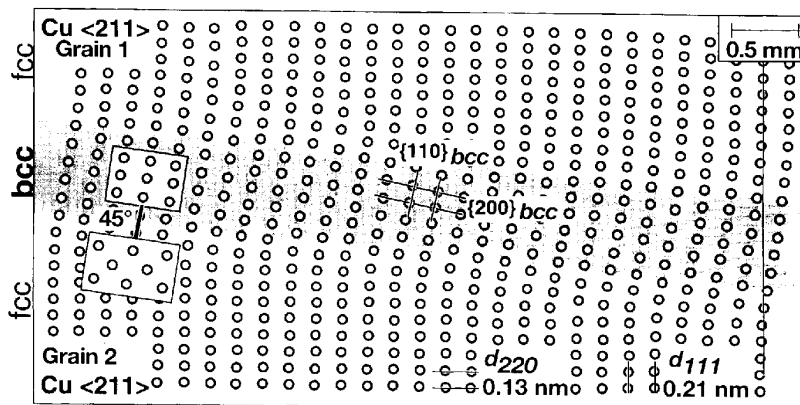

Fig. 11. Model of the $\Sigma 3$ 84° $\langle 211 \rangle$ tilt boundary, calculated by molecular dynamics [24, 25, 47]. The calculations predict that the boundary contains a thin slab ($\approx$ 1 nm in width) of Cu with the bcc structure of α-Fe (A2 in Pearsons's notation [44]). The inset shows the structure after rotating it by 45° around an axis parallel to the close-packed layers and parallel to the image plane. In this inset the viewing direction corresponds to $\langle 100 \rangle_{bcc}$.
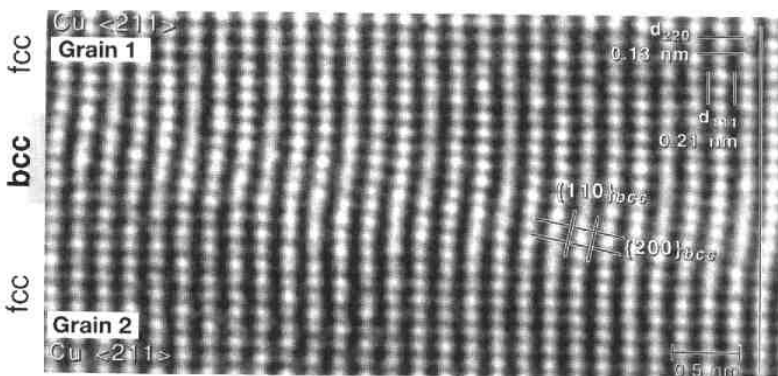

Fig. 12. Experimental HRTEM image of the Cu $\Sigma 3$ 84° $\langle 211 \rangle$ tilt boundary, which corresponds to Fig. 1f [6, 7]. The viewing direction coincides with the $\langle 211 \rangle$ tilt axis. This image has been recorded in the same microscope as the images in Figs. 6 and 7, however with a side-entry objective lens reaching a point resolution of 0.12 nm [11]. The image agrees well with the result of molecular dynamics modeling in Fig. 11, according to which the boundary contains a thin slab of Cu with the bcc structure of α-Fe.

with the fcc stacking of close-packed layers and regions where the stacking sequence corresponds to the 2H structure, a hexagonal close-packed structure of the Mg type (A3 in Pearson's notation [44]). The outer regions of the slab, however, fully preserve their bcc structure. Further details will be published elsewhere [51].

4.3 Structures Observed by HRTEM

Figure 12 presents an experimental HRTEM image of the $\Sigma 3$ 84° $\langle 211 \rangle$ tilt boundary in Cu [24, 25]. The image is part of a focus series and has been recorded near Scherzer focus in an ultrathin region of the TEM foil. The local foil thickness does not exceed 10 nm, according to an image obtained after tilting the foil by 30° around an axis parallel to the boundary and normal to the projection. Computer-simulated HRTEM images indicate that under these conditions the positions of Cu columns coincide with those of the dark intensities in the HRTEM image. We emphasize, however, that the conclusions to be drawn below do not depend on the details of the correspondence between the projected structure and its HRTEM image.

The simultaneous resolution of {111} and {220} planes in both grains in Fig. 12 and the exact parallelism of the {111} planes indicates that the orientation relationship does not deviate by more than 1° from $\Sigma 3$. The inclination of the boundary plane in Fig. 12 amounts to $\phi_{211} \approx 85°$, in good agreement with the macroscopic boundary inclination. Therefore, the crystallographic parameters of the diffusion-bonded bicrystal studied in our experiments match very well with those underlying the molecular dynamics calculations.

Similar to the calculated structure in Fig. 11, the HRTEM image of Fig. 12 exhibits an extended zone of distortion along the boundary. The {111} atomic layers of the two bulk crystals bend where they cross the boundary. This is seen more easily in Fig. 12 when comparing the course of the {111} fringes with the vertical straight line on the right. From Fig. 12 we have obtained a preliminary structure model by applying the above method of cross-correlating the experimental image with the contrast pattern of a single column of Cu atoms. Figure 13 compares the result with the structure of Fig. 11 predicted by molecular dynamics calculations. While an iterative structure refine-
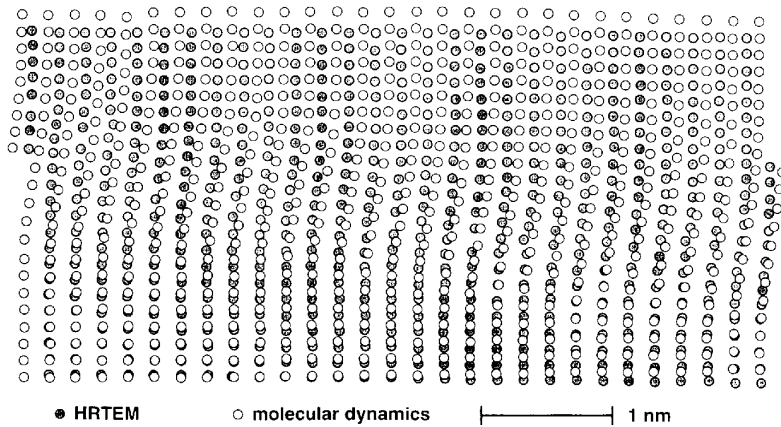

● HRTEM   ○ molecular dynamics |————————| 1 nm

Fig. 13. Comparison between the (unrefined) experimental structure (dark balls) and the theoretical structure (white balls) of the $\Sigma 3$ 84° $\langle 211 \rangle$ tilt boundary in Cu. The two models have been positioned to match at the bottom left corner.
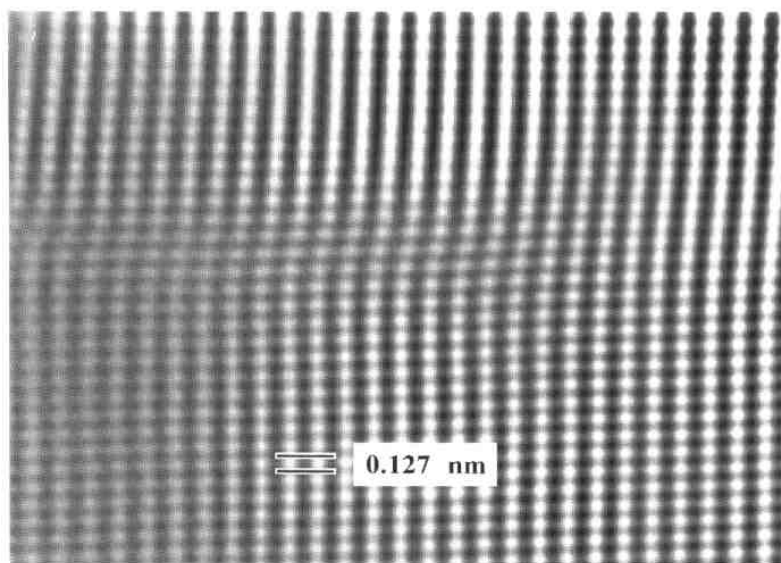

0.127 nm

Fig. 14. Television image of the $\Sigma 3$ 84° $\langle 211 \rangle$ tilt boundary at 900 K, recorded with the JEM-ARM 1250 (side-entry stage). By means of digital image processing we have reduced the noise and enhanced the contrast. This image confirms that the grain boundary slab with the bcc structure persists at high temperatures. The slab has a thickness of about 1 nm, which does not differ much from the slab thickness observed at room temperature (Fig. 12).

ment has not been carried out yet, the real structure exhibits significant discrepancy with the computer-simulated structure: The model obtained by molecular dynamics calculations overestimates the width of the bcc zone and the inclination of the {110}$_{bcc}$ planes against the {111}$_{fcc}$ planes. Consequently, the calculations expect the offset between corresponding {111}$_{fcc}$ planes across boundary to be twice as large as in the real structure. Structure refinement will not resolve these discrepancies; from the analysis of the Σ3 90° ⟨110⟩ tilt boundary we estimate that structure refinement corrects the preliminary column positions by no more than 0.02 nm.

Figure 14 presents a first image of the Σ3 84° ⟨211⟩ tilt boundary at 900 K. Owing to a pronounced specimen drift at this high temperature we had to record the image of Fig. 14 with the television system attached to the JEM-ARM 1250. To correct for the inferior quality of the TV image we have reduced the noise and enhanced the contrast of the image. After noise reduction and contrast enhancement the image clearly reveals the {111} and {220} spacings of Cu, like Fig. 12 does at room temperature. Figure 14 confirms that the grain boundary slab of bcc Cu also exists at elevated temperatures. So far, however, we have no experimental evidence for the oscillations of the slab width one would except according to the molecular dynamics calculations. Moreover, the image suggests that the slab thickness at 900 K does not substantially exceed the slab thickness at room temperature (compare Fig. 14 with Fig. 12). Again, this result disagrees with the predictions of our molecular dynamics calculations. However, we must point out that the image of Fig. 14 suffers from two problems: (i) The orientation relationship of the bicrystal deviates significantly more from Σ3 than in the bicrystal of Fig. 12. (ii) Owing to the high evaporation rate of the TEM specimen at 900 K we have not yet succeeded in imaging the same region at room temperature and 900 K. For these regions, the image of Fig. 14 constitutes a preliminary result and further experiments are required before we can finally prove or disprove the hypothesis of slab broadening at high temperature.

5 Discussion

For a simple orientation relationship like Σ3 one might expect particularly simple grain boundary structures, for which the coherent twin boundary constitutes a well-known example. However, the experimental and theoretical data we have presented here reveals that Σ3 tilt boundaries in Cu have a particularly complex structure when the inclination approaches 90° against the {111} plane of the coherent twin boundary. In the following we focus on the common features of the Σ3 ⟨110⟩ and Σ3 ⟨211⟩ tilt boundaries with high inclination. For a discussion of aspects special to either one type of tilt boundary we refer the reader to previous publications [18 to 22, 24, 25, 46, 47].

The excellent agreement between HRTEM images and computer-generated models on the one side and the agreement between calculated and measured energies on the other side confirm that the observed structures represent in fact the most stable atom configurations under the respective conditions. For both families of Σ3 tilt boundaries the HRTEM images and computer-generated models agree on a

number of features, which appear to be rather unusual: (i) At high inclinations against the coherent twin boundary the grain boundaries constitute three-dimensional rather than two-dimensional crystal defects. (ii) The corresponding atom arrangements have a lower symmetry than the 'macroscopic' symmetry of the bicrystals would allow for. (iii) In the volume of the slab that characterizes these boundaries, Cu adopts unusual crystal structures: 9R and A2 (bcc) or A3 (hcp).

The Σ3 orientation relationship guarantees that the two grains have one set of close-packed layers parallel to each other. At the boundary plane, however, these layers cannot match each other because they meet with opposite stacking sequences: ...abcabc... in one grain versus ...cbacba... in the other grain. Formally, one can transform the fcc structure into 9R or hcp by sliding those close-packed {111} layers over each other in order to change their stacking sequence. Similarly, sliding and straining those close-packed layers transforms the fcc structure into the bcc structure and converts the close-packed {111} layers of the fcc structure into the close-packed {110} layers of the bcc structure. Thus, while the three 'alternative' structures of the boundary slab differ in crystal symmetry, they have one feature in common: They continue closed-packed {111} layers of the fcc structure across the grain boundary – even though this requires to 'slide' these layers laterally against each other.

Continuation of close-packed layers seems to be energetically favorable, irrespective of the stacking sequence. We conclude that the 9R and bcc (or, at high temperatures, hcp) structures form as a compromise combining continuation of close-packed layers with good matching between layers that have different stacking positions in the two grains.

Concerning the width of the boundary slab, we propose that mechanical equilibrium requires balancing of two energy terms with opposite dependencies on the slab width. The first energy term corresponds to an elastic repulsion between the two slab/grain interfaces – the interfaces that the boundary slab makes with the adjacent grains. The repulsion reflects the energy that would be required to replace the two interfaces by a single boundary, which would have high energy because of reversing the stacking sequence abruptly. The exponential stress-distance dependence of small angle grain boundaries [52] suggests that one may model the repulsion between the slab/grain interfaces by an energy term that decreases exponentially with increasing width of the boundary slab [22]. The second energy term corresponds to the energy increase associated with the excess energy the slab structures has over the fcc structure. This term increases proportional to the width of the boundary slab, thus corresponds to an attraction between the two slab/grain interfaces.

Since the boundary slabs we observe have a substantial width the energies of the corresponding 'alternative' crystal structures cannot significantly exceed the energy of the fcc structure. In fact, we know from ab initio calculations on Cu that the energy difference between the fcc structure (ground state) and the 9R structure or the hcp structure is rather small [43]. Likewise, the energy of bcc Cu is not substantially higher than the energy of fcc Cu [53, 54]. Experimental observations confirm that the respective energy differences are not too large: Cu with 9R structure has been observed in the form of precipitates in Fe-Cu and Fe-Cu-Ni

alloys [55], while epitaxy of Cu on α-Fe [56] or precipitation of Cu in an α-Fe matrix [57, 58] yields Cu with the bcc structure.

Because these arguments are quite general, one may expect grain boundary structures similar to those we have discussed here also in other fcc metals with low stacking fault energy. In fact, Σ3 ⟨110⟩ tilt boundaries with 9R structure have also been observed in Ag [22, 46, 59] (including the characteristic variation of the boundary energy with inclination angle [60]) and Au [61].

While the HRTEM images and computer-modeled structures agree on the characteristic features of the grain boundaries, discrepancies remain concerning the precise positions of atoms or atom columns. For the Σ3 84° ⟨211⟩ tilt boundary these discrepancies are relatively large. On the other hand, the significance of the discrepancies is rather low because the structure obtained by molecular dynamics relaxations exhibit substantial variation themselves. The reason for these variations lies in the rather long period of the grain boundary structure and in the relatively complex interaction with secondary defects [47].

For the Σ3 ⟨110⟩ tilt boundaries the calculated structures are unique, and thus the discrepancies with the experimentally observed atom positions appear to be more significant. According to Fig. 9 the semi-empirical Finnis-Sinclair potential employed in the molecular statics calculations underestimates the width of the 9R slab. A similar result is even found with the embedded-atom potential, although this potential predicts a stacking fault energy substantially smaller than in reality. This implies that the calculations do not correctly reproduce the repulsive interaction between the small angle and the large angle boundary, either. The reason for this may be that the potential underestimates the repulsive forces between two atoms closer than the next neighbor distance in Cu.

This work presented here shows that the energy and the structure of twin boundaries in Cu sensitively depend on the boundary inclination. In particular, both inclination dependencies of the grain boundary energy (Figs. 3 and 10) exhibit a second minimum besides the minimum corresponding to the coherent twin boundary.

It is well known that grain boundaries of minimum energy occur for orientation relationships exactly at or close to low-Σ orientation relationships and at particular inclinations of the boundary plane [1, 2, 7 to 13]. An important difference exists, however, between the roles that the orientation relationship and the boundary plane inclination play in the formation of energetically favorable grain boundaries in polycrystals: diffusion can change the inclination of a grain boundary, but not the orientation relationship between adjacent grains (except for extremely small grains, which may rotate).

Evidence for pronounced effects of the grain boundary inclination has recently been obtained from experimental observations on grain boundary phase transitions [14]. In those experiments, the energy minimum at a low-Σ orientation relationship has been observed to disappear above a critical temperature T_C and at the same temperature the grain boundary also looses other 'special' properties. These observations have been interpreted in terms of a faceting transformation, in which a grain boundary with high energy dissociates into facets with low energy. In fact, such faceting phase transitions have been experimen-

tally observed in Cu [42, 48, 62] and Ag [60]. In both metals, twin boundaries with random inclinations were observed to dissociate into facets of coherent twin boundary and facets whose inclinations correspond to the above boundaries with either the 9R or the bcc structure. The facets forming on Σ3 ⟨110⟩ tilt boundaries in Cu [39] and Ag [37] have nearly the same geometry.

Again, this suggests that the alternative structures observed in Cu Σ3 tilt boundaries can also form in other fcc metals.

It has been established that with varying orientation relationship kinetic properties of grain boundaries, like diffusivity or mobility, vary in the same sense as the grain boundary energy but even more pronounced [1, 2, 14, 48]. Evidence for strong variation of kinetic properties has been obtained, for example, for the Σ86 ⟨1120⟩ tilt boundary in Zn [15]. Varying the inclination of this boundary changes its mobility over three orders of magnitude. Therefore, we expect that the strong inclination dependence of the grain boundary energy and structure we have observed for Cu twin boundaries goes along with even stronger variations of kinetic properties of these grain boundaries.

Literature

1. Sutton, A.P.; Balluffi, R.W.: Interfaces in Crystalline Materials, Clarendon Press, Oxford (1995).
2. Gleiter, H.; Chalmers, B.: "High Angle Grain Boundaries", in: B. Chalmers, J.W. Christian, T.B. Massalski (eds.), Progress in Materials Science, Pergamon Press, Oxford (1972) 1–272.
3. Kronberg, M.L.; Wilson, F.H.: Trans. AIME 185 (1949) 501–514.
4. Sutton, A.P.; Vitek, V.: Trans. Roy. Soc. London A 309 (1983) 1–6.
5. Sutton, A.P.; Vitek, V.: Trans. Roy. Soc. London A 309 (1983) 55–63.
6. Sutton, A.P.; Vitek, V.: Trans. Roy. Soc. London A 309 (1983) 37–42.
7. Wolf, D.: Acta Metall. 37 (1989) 1983–1993.
8. Wolf, D.: Acta Metall. 37 (1989) 2823–2833.
9. Wolf, D.: Acta Metall. 38 (1990) 781–790.
10. Wolf, D.: Acta Metall. 38 (1990) 791–798.
11. Gjostein, N.A.; Rhines, F.N.: Acta Metall. 7 (1959) 319–330.
12. Miura, H.; Kato, M.; Mori, T.: J. Physique 51 (1990) C1-263–268.
13. Hasson, G.; Goux, C.: Scripta metall. 5 (1971) 889–894.
14. Maksimova, E.L.; Shvindlerman, L.S.; Straumal, B.B.: Acta Metall. 36 (1988) 1573–1583.
15. Straumal, B.B.; Sursaeva, V.G.; Shvindlerman, L.S.: Phys. Met. Metall. 49 (5) (1980) 102–107.
16. Omar, R.: "Grain Boundary Energies in Copper", Ph. D. thesis, University of Warwick (1987).
17. Schmelzle, R.; Muschik, W.; Gust, W.; Predel, B.: Scripta metall. mater. 25 (1991) 1981–1986.
18. Wolf, U.; Ernst, F.; Muschik, T.; Finnis, M.W.; Fischmeister, H.F.: Phil. Mag. A 66 (1992) 991–1016.
19. Wolf, U.; Ernst, F.; Muschik, T.; Finnis, M.W.; Fischmeister, H.F.: "The Influence of Grain Boundary Inclination on the Structure and Energy of Σ3 Twin Boundaries in Copper", in: W.A.T. Clark, C.L. Briant, U. Dahmen (eds.), Structure and Properties of Interfaces in Materials, Materials Research Society, Pittsburgh (1992) 177–182.

20. *Ernst, F.; Hofmann, D.; Nadarzinski, K.; Stemmer, S.; Streiffer, S.K.:* "Quantitative high-resolution electron microscopy of Interfaces", in: A.C. Ferro, E.P. Conde, E.A. Fortes (eds.), Intergranular and Interphase Boundaries in Materials, Trans Tech Publications, Zürich (1996) 23–34.

21. *Hofmann, D.; Ernst, F.:* Ultramicroscopy *53* (1994) 205–221.

22. *Hofmann, D.; Ernst, F.:* Interf. Sci. *2* (1994) 201–210.

23. *Möbus, G.; Ernst, F.:* "Determination of interface structures by quantitative interpretation of HREM images", in: J. Heydenreich, W. Neumann (eds.), Electron Microscopy of Boundaries and Interfaces in Materials Science, Elbe, Wittenberg (1995), 61–70.

24. *Schmidt, C.; Ernst, F.; Finnis, M.W.; Vitek, V.:* Phys. Rev. Lett. *75* (1995) 2160–2163.

25. *Schmidt, C.; Finnis, M.W.; Vitek, V.; Ernst, F.:* "Simulation of a layer of bcc copper in the Σ3-82° ⟨211⟩ tilt boundary and its confirmation by high resolution transmission electron microscopy", in: A.C. Ferro, E.P. Conde, E.A. Fortes (eds.), Intergranular and Interphase Boundaries in Materials, Trans Tech Publications, Zürich (1996) 337–340.

26. *Bridgman, P.W.:* Proc. Am. Ac. Arts. Sci. *58* (1923) 163.

27. *Mullins, W.W.:* J. Appl. Phys. *28* (1957) 333–339.

28. *Mullins, W.W.:* "Solid surface morphologies governed by capillarity", in: Metal Surfaces: Structure, Energetics and Kinetics, American Society for Metals, Metals Park (1963) 17–66.

29. *Herring, C.:* "Surface tension as a motivation for sintering", in: W.E. Kingston (ed.) The Physics of Powder Metallurgy, McGraw-Hill, New York (1951) 143–179.

30. *Tolmon, F.R.; Wood, J.C.:* J. Sci. Instr. *33* (1956) 263–241.

31. *Phillipp, F.; Möbus, G.; Rühle, M.:* Ultramicroscopy *56* (1994) 1–10.

32. *Stadelmann, P.A.:* Ultramicroscopy *21* (1987) 131–145.

33. *Nadarzinski, K.; Ernst, F.:* "Quantitative HRTEM of the Σ3 (111) Grain Boundary in NiAl", in: A.C. Ferro, E.P. Conde, E.A. Fortes (eds.), Intergranular and Interphase Boundaries in Materials, Trans Tech Publications, Zürich (1996) 309–312.

34. *Nadarzinski, K.; Ernst, F.:* Phil. Mag. A, in press.

35. *Kienzle, O.; Ernst, F.:* J. Am. Ceram. Soc., submitted.

36. *Möbus, G.; Necker, G.; Rühle, M.:* Ultramicroscopy *49* (1993) 46–65.

37. *Foiles, S.M.; Baskes, M.I.; Daw, M.S.:* Phys. Rev. B *33* (1986) 7983–7991.

38. *Finnis, M.W.; Sinclair, J.E.:* Phil. Mag. A *50* (1984) 45–55.

39. *Foreman, A.J.E.; English, C.A.; Phythian, W.J.:* Phil. Mag. A *66* (1992) 655–669.

40. *Ackland, G.J.; Tichy, G.; Vitek, V.; Finnis, M.W.:* Phil. Mag. A *56* (1987) 735–756.

41. *Wolf, U.:* "Atomistische Simulation von Grenzflächen in kubisch-flächenzentrierten Übergangsmetallen", Dissertation, Universität Stuttgart (1991).

42. *Laub, W.:* "Zweikristallexperimente zur Untersuchung der Energie und Stabilität von Cu-Σ3-Korngrenzen", Dissertation, Universität Stuttgart (1993).

43. *Ernst, F.; Finnis, M.W.; Hofmann, D.; Muschik, T.; Schönberger, U.; Wolf, U.; Methfessel, M.:* Phys. Rev. Lett. *69* (1992) 620–623.

44. *Pearson, W.B.:* A Handbook of Lattice Spacings and Structures of Metals and Alloys, Pergamon Press, London (1958) 85.

45. *Ždahnov, G.S.; Minervina, Z.V.:* Zh. Eksperim. Theoret. Fiz. *17* (1947) 3.

46. *Hofmann, D.:* "Quantitative Hochauflösungselektronenmikroskopie an Zwillingskorngrenzen in kfz Metallen", Dissertation, Universität Stuttgart (1994).

47. *Schmidt, C.:* "Atomistische Computersimulation der Energie und Struktur von symmetrischen und asymmetrischen Σ3-Kippkorngrenzen in Kupfer", Dissertation, Universität Stuttgart (1996).

48. *Laub, W.; Oswald, A.; Muschik, T.; Gust, W.; Fournelle, R.A.:* "The faceting transformation of Σ3 grain boundaries in copper", in: W.C. Johnson et al. (eds.), Solid-Solid Phase Transformations, Minerals. Metals & Materials Society, Warrendale (1994) 1115–1120.

49. *Andersen, H.C.:* J. Chem. Phys. *72* (1980) 2384–2393.

50. *Parrinello, M.; Rahman, A.:* J. Appl. Phys. *52* (1981) 7182–7190.

51. *Schmidt, C.; Finnis, M.W.; Vitek, V.:* in preparation.

52. *Hirth, P.; Lothe, J.:* The Theory of Dislocations, Wiley, New York (1982).

53. *Paxton, A.T.; Methfessel, M.; Polatoglou, H.M.:* Phys. Rev. B *41* (1990) 8127–8132.

54. *Kraft, T.; Marcus, P.M.; Methfessel, M.; Scheffler, M.:* Phys. Rev. B *48* (1993) 5886–5890.

55. *Othen, P.J.; Jenkins, M.L.; Smith, G.D.W.; Phythian, W.J.:* Phil. Mag. Lett. *64* (1991) 383–391.

56. *Celinski, Z.; Heinrich, B.; Cochran, J.F.; Myrtle, K.; Arrot, A.S.:* "Ferromagnetic resonance studies of BCC epitaxial ultrathin Fe(001)/Cu(001) bilayers and Fe(001)/Cu(001)/Fe(001) trilayers", in: G.C. Hadjipanayis, G.A. Prinz (eds.), Science and Technology of Nanostructured Magnetic Materials, Plenum Press, New York (1991) 77–80.

57. *Goodman, S.R.; Brenner, S.S.; Low, J.R.:* Met. Trans. A *4* (1973) 2363–2369.

58. *Goodman, S.R.; Brenner, S.S.; Low, J.R.:* Met. Trans. *4* (1973) 2371–2378.

59. *Hofmann, D.; Finnis, M.W.:* Acta Metall. Mater. *42* (1994) 3555–3567.

60. *Barg, A.I.; Rabkin, E.; Gust, W.:* Acta Metall. Mater. *43* (1995) 4067–4074.

61. *Ichinose, H.; Ishida, Y.; Baba, N.; Kanaya, K.:* Phil. Mag. A *52* (1985) 51–59.

62. *Muschik, T.; Laub, W.; Wolf, U.; Finnis, M.W.; Gust, W.:* Acta Metall. *41* (1993) 2136–2171.